JOURNAL OF SOLID STATE CHEMISTRY 70, 129–136 (1987)

A New Structure Type in the Bi_2O_3–Nb_2O_5 System*

W. ZHOU, D. A. JEFFERSON, AND J. M. THOMAS†

Department of Physical Chemistry, University of Cambridge, Lensfield Road, Cambridge CB2 1EP, United Kingdom

Received January 13, 1987; in revised form March 30, 1987

Solid solutions of Bi_2O_3 and Nb_2O_5 encompassing the compositional range from pure Bi_2O_3 to $5Bi_2O_3 \cdot 3Nb_2O_5$ exhibit a range of complicated ordered structures which are extremely difficult to study by X-ray diffraction methods. High resolution electron microscopy, using previously outlined methodologies, has proved capable of elucidating the structural principles upon which the so-called Type III phase, with a composition of approximately $7Bi_2O_3 \cdot 3Nb_2O_5$, is based. The structure of this phase is a composite one, built up of limited fluorite, pyrochlore, and perovskite units. © 1987 Academic Press, Inc.

Introduction

We welcome this opportunity of dedicating this contribution to Professor Jellinek, whose numerous and wide-ranging studies have constituted important landmarks in the elucidation of complicated solid structures, especially those of metal chalcogenides. Jellinek and his co-workers were particularly successful in clarifying the structural principles of transition metal sulphides by X-ray powder diffraction methods. The systems which we are currently investigating (*1–3*), namely the ternary oxides Bi_2O_3–Nb_2O_5, Bi_2O_3–Ta_2O_5, Bi_2O_3–MoO_3, and Bi_2O_3–WO_3, are however not so readily amenable to powder diffraction methods and alternative lines of inquiry have been invoked. We have found that high resolution electron microscopy has proved the most successful, and we report here the results of a typical structural study.

The system Bi_2O_3–Nb_2O_5, first studied by Roth and Waring (*4*), using X-ray powder diffraction methods, has recently been shown to contain a series of hitherto unknown phases in the composition field between pure Bi_2O_3 and $5Bi_2O_3 \cdot 3Nb_2O_5$. These phases, which lie in what was previously designated as a continuous solid solution with a fluorite structure, are of four types, were identified by electron diffraction, and the structures of two of them have been determined using high resolution electron microscopy (HREM).

The simplest phase is that designated Type I, centered at a composition $15Bi_2O_3 \cdot Nb_2O_5$, and includes niobium ordering in a body-centered cubic unit cell with a repeat length twice that of the basic fluorite cell. The exact arrangement of oxygen vacancies is the subject of a current investigation, but is thought to be similar to that of β-Bi_2O_3 (*5*).

The Type II phase is considerably more

* Dedicated to Dr. Franz Jellinek.

† Present address: Davy Faraday Research Laboratory, The Royal Institution, 21 Albemarle Street, London W1X 4BS, England.

0022-4596/87 $3.00

complex, existing in the composition range from $12Bi_2O_3 \cdot Nb_2O_5$ to $4Bi_2O_3 \cdot Nb_2O_5$, and exhibits an incommensurate cubic unit cell with a side of at least 44 Å. A scheme of niobium ordering onto the {111} planes of the unit cell was determined from the HREM images, and an acceptable oxygen vacancy ordering scheme was found by incorporating pylochlore-like coordination around the niobium atoms, with the bismuth in a defect fluorite environment. Similar phases to these have now been found in the systems Bi_2O_3–V_2O_5 and Bi_2O_3–Ta_2O_5 (*3*), and some of these materials have shown promising potential catalytic activity (*6*).

Of the remaining two phases in the Bi_2O_3–Nb_2O_5 system, that designated Type IV, with a composition on or around $5Bi_2O_3 \cdot 3Nb_2O_3$, has been previously studied by HREM (*7*) and has been tentatively assigned to a structure based upon a regular intergrowth of Aurivillius-like phases (*8*). Current investigations suggest that the structure is more complex but is almost certainly perovskite-based, and lies outside the range of the fluorite-based phases. The other phase, designated Type III, is clearly fluorite-based, but was shown to be a layered phase, possibly combining some of the features of both the Type II and IV phases. Accordingly, a full structural investigation of this phase was undertaken to ascertain how the basic fluorite structure copes with increasing niobium contact.

Experimental

Samples were prepared by direct solid state reaction of the component oxides in oxygen at 800°C. These were examined initially by X-ray powder diffractometry and the stoichiometry checked using X-ray microprobe analysis in the electron microscope. HREM examination was carried out in a JEOL JEM-200CX electron microscope operating at 200 kV, fitted with a double-tilt/lift stage, the operating characteristics of the instrument being such that a point resolution of 2.4 Å was readily attainable. Optimum results were achieved by recording images at 500,000× at an objective lens underfocus slightly greater than the optimum value (*9*), objective lens astigmatism being corrected by observing the granularity of the amorphous carbon support film. Image simulations from model structures were carried out by the multislice method (*10, 11*) using computer programs written by one of us (DAJ) for a previous study in the system Bi_2O_3–MoO_3–WO_3 (*12*).

Results and Discussion

The X-ray powder diffraction diagram of the Type III phase is shown in Fig. 1. The basic lines are clearly those of a fluorite-like phase, in accordance with a recent study (*13*) although additional lines can be seen, indicating a superlattice. The three principle electron diffraction patterns from this phase are shown in Figs. 2a–2c, taken down the [100], [110], and [001] axes of the fluorite subcell. These are indicative of a face-centered tetragonal structure with two threefold and one sevenfold repeat on the basic fluorite lattice: alternatively with the two threefold axes rotated by 45° a more conventional body-centered tetragonal cell with $a = b = 11.7$ Å, $c = 38.5$ Å results. X-ray microanalysis indicated that the structure giving these diffraction patterns could be found at the composition $3Bi_2O_3 \cdot Nb_2O_5$. By the time the composition $2Bi_2O_3 \cdot Nb_2O_5$ was reached, the Type IV structure, or a variant of it, predominated, but at a composition approximating to $17Bi_2O_3 \cdot 8Nb_2O_5$, a variant of the Type III structure, but with a disordered repeat in the direction of the long axis, was found. The characteristic diffraction pattern from this phase is shown in Fig. 2d.

HREM images correspond to the diffrac-

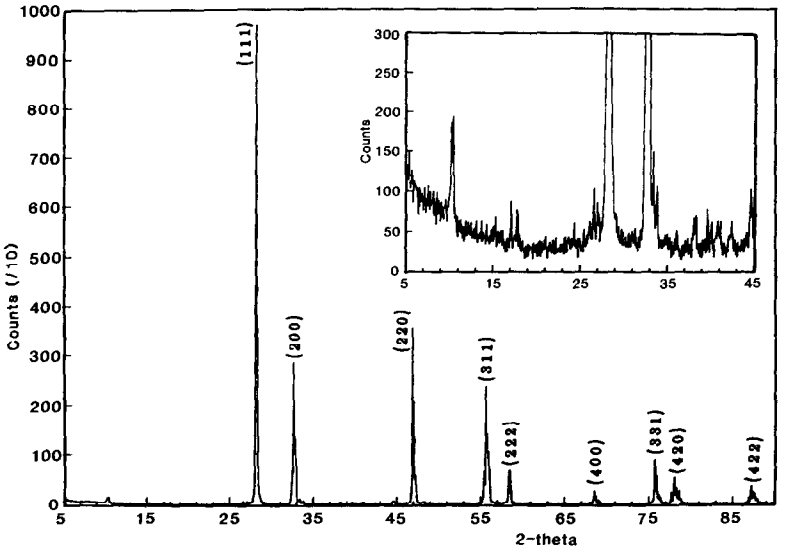

FIG. 1. X-ray powder diffraction pattern of the Type III phase, with the composition $3Bi_2O_3 \cdot Nb_2O_5$. The lines are indexed according to a simple fluorite structure. The inset trace shows one portion of the pattern at an increased vertical scale, when superlattice lines are evident.

tion patterns Fig. 3. When viewed down the [100] axis of the fluorite sub cell, the 3 × 7 superlattice was just visible (Fig. 3a). Similarly, the 3 × 3 superlattice was present in images viewed down the fluorite [001] axis, but the image contrast was generally devoid of features and gave little indication of the true nature of the superstructure (Fig. 3b). When viewed down fluorite [110], however, considerable detail was revealed, as in the case of the Type II structure described previously, and a characteristic diagonal pattern of rows of white dots was readily discernible (Fig. 3c). Close examination of the image contrast revealed that the structure was clearly layer-like, with the component layer being 3.5 fluorite unit cells in thickness: two of those layers, offset by a vector equal to 1.5 times the length of a face-diagonal of the fluorite subcell make up the 3 × 3 × 7 superstructure. In the $17Bi_2O_3 \cdot 8Nb_2O_5$ structure the basic arrangement is similar (Fig. 3d) but the new layer appears to be some five fluorite subcells in thickness: in this phase, however, the structure is not ordered, and these thicker layers are interspersed with the more normal layers characteristic of the $3Bi_2O_3 \cdot Nb_2O_5$ composition.

Analysis of the HREM images proceeded in a similar manner to that of the Type II structure (*1*), using mainly the [110] projected images. In an analogous manner to this structure and to the basic pyrochlore arrangement, the image shows little contrast in the thinner parts at the margins of the crystal, merely a diamond-shaped network of dots representing the cation positions, but as the crystal thickness increases a distinct pattern emerges, with multiple scattering producing some rows of dots with lighter contrast than their neighbors. In both pyrochlore and the Type II structure this could be used to construct a model for the pattern of bismuth/niobium ordering: accordingly, models could be devised for the Type III structure on the basis that this assumption remained valid. When the

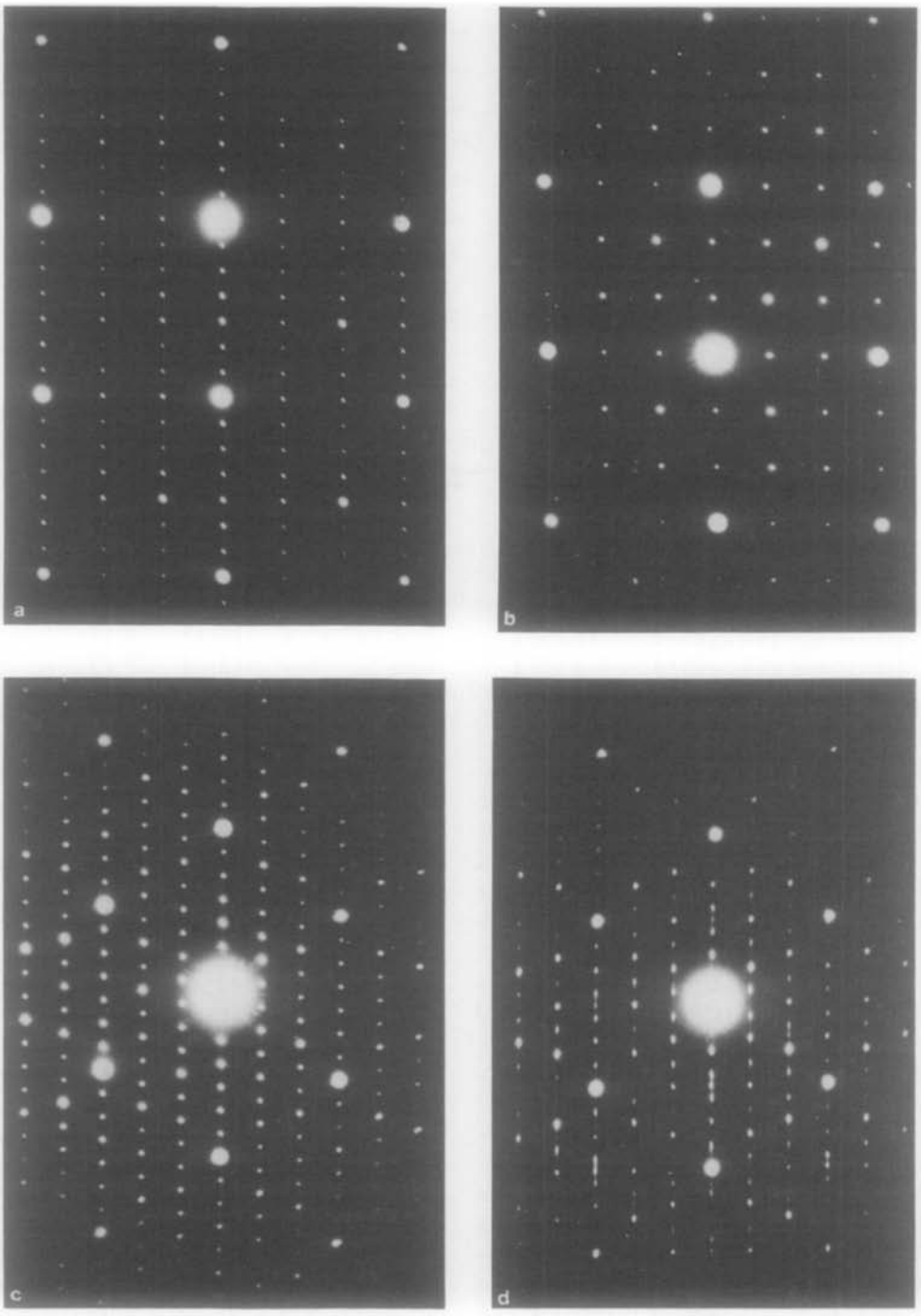

FIG. 2. Selected area electron diffraction patterns of crystals of the Type III phase, viewed down (a) the [100], (b) [001], and (c) [110] axes of the fluorite subcell. (d) shows the [110] patterns of the modified Type III structure with disorder in the [100] direction. (In all cases subcell maxima corresponding to the fluorite subcell are much stronger than average.)

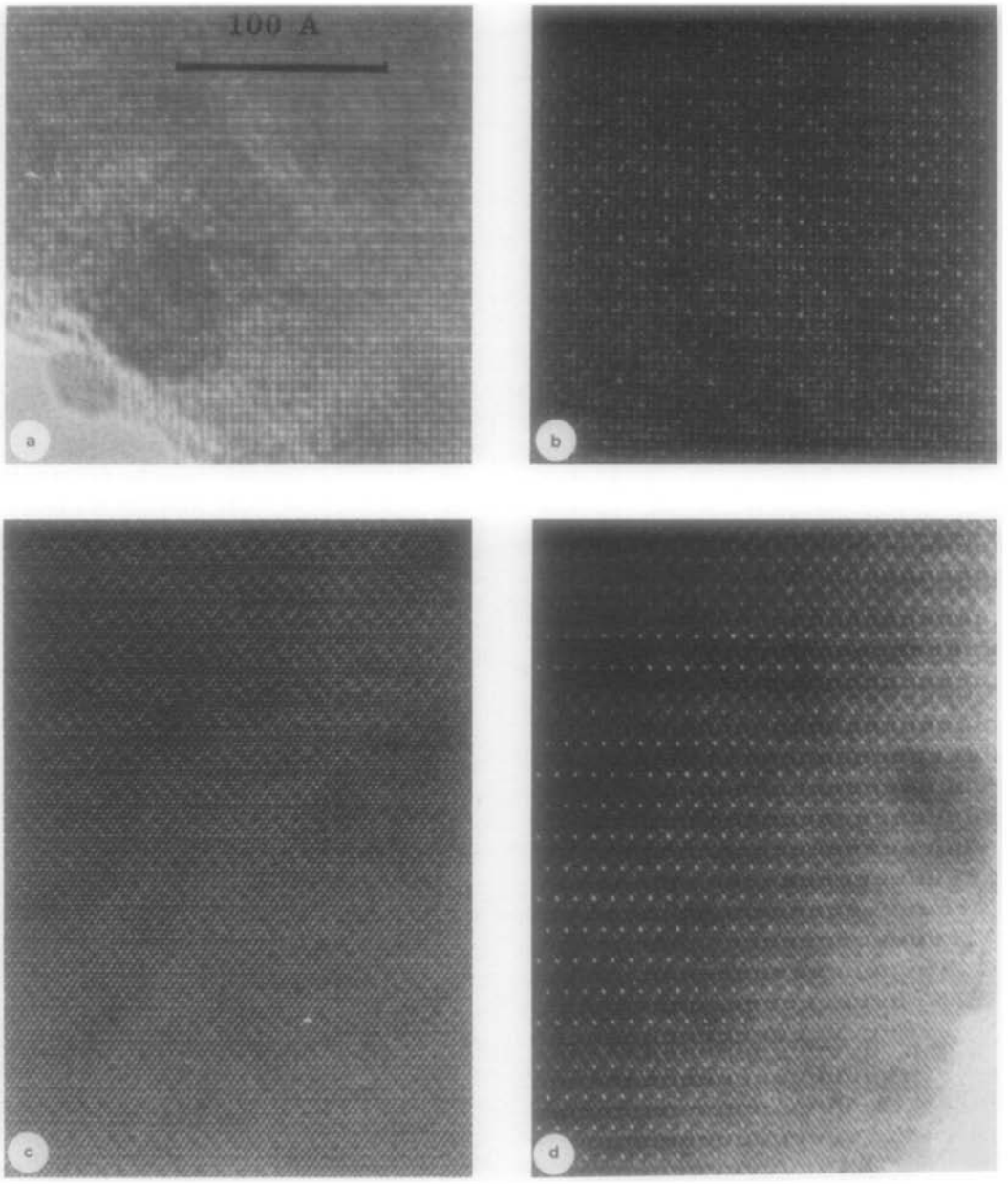

FIG. 3. HREM images corresponding to the selected area electron diffraction patterns of Fig. 2. In (d), the presence of units some five fluorite subcells in thickness is clearly visible (arrowed), as is the lack of offset of the prominent white dots (all micrographs are at the same magnification).

known stoichiometry of the material was taken into account, only one model gave a suitable image match at all conditions of specimen thickness and defocus, with a projected cation arrangement closely matching the diamond-shaped pattern of contrast visible in the image and a calculated cation ratio of 44Bi : 19Nb, lying

within the composition range observed for the Type III phase.

As with the previous structures in this system, the derivation of the cation arrangement is only a part of a trial structure elucidation. With the resolution available, neither the oxygen atoms nor small displacements of the cations are experimentally determinable: consequently they must be inferred from the cation arrangement, bearing in mind the known coordination preferences of bismuth and niobium and the number of oxygen vacancies required to achieve the desired stoichiometry. In the Type II structure the observed images and stoichiometry could be explained purely in terms of elements of the fluorite and pyrochlore structures: with the Type III phase a model based on these two structural elements only was constructed but showed serious shortcomings.

In particular, the model required that octahedra within adjacent pyrochlore units must share not only corners but also edges if the threefold repeat of the basal plane of the unit cell was to be maintained: this was incompatible with any conventional derivative of the pyrochlore structure, which of necessity includes an even multiple of the basic fluorite subcell. Furthermore, with this initial model it was impossible to achieve the correct number of oxygen vacancies as the niobium content of Type III was much higher than in the Type II structure. Consequently, a different type of structural element was required.

The only simple way to overcome the deficiencies of a model based totally on fluorite and pyrochlore units is to remove the necessity for two pyrochlore units to exist in adjacent subcells. An indication of how this may be done is illustrated in Fig. 4. First, the niobium atom common to the two pyrochlore units is replaced by bismuth, as indicated. (This may be done without a serious change to the overall stoichiometry.) Then the NbO_6 octahedra

FIG. 4. The final structural model for the Type III structure, projected down the [110] fluorite direction. The bismuth atoms replacing the niobium atoms of the initial pyrochlore units are shown as filled black circles situated above and below the fourfold rings of octahedra which constitute the perovskite units. For clarity, the fluorite part of the structure filling the spaces in the framework is omitted.

which share edges are rotated about their axes perpendicular to the shared edges, introducing additional oxygen atoms, which reduces the number of oxygen vacancies, and creates what is effectively a fourfold ring of corner sharing octahedra reminiscent of those found in perovskite. A complete layer of the structure is then built up by alternating pyrochlore and perovskite units in this way, as shown, and the spaces in the framework so created can be filled with bismuth and oxygen in a defect fluorite environment. The overall composition of this structure is $Bi_{86}Nb_{40}O_{29}$, which agrees well with that observed experimentally, and the closeness of the match between real and simulated images is shown in Fig. 5. Furthermore, the model can be extended readily to cope with the longer-period structure observed in Fig. 3d, merely by adding a further layer of perovskite and pyrochlore structural units. On the basis that the complete "layers" are separated

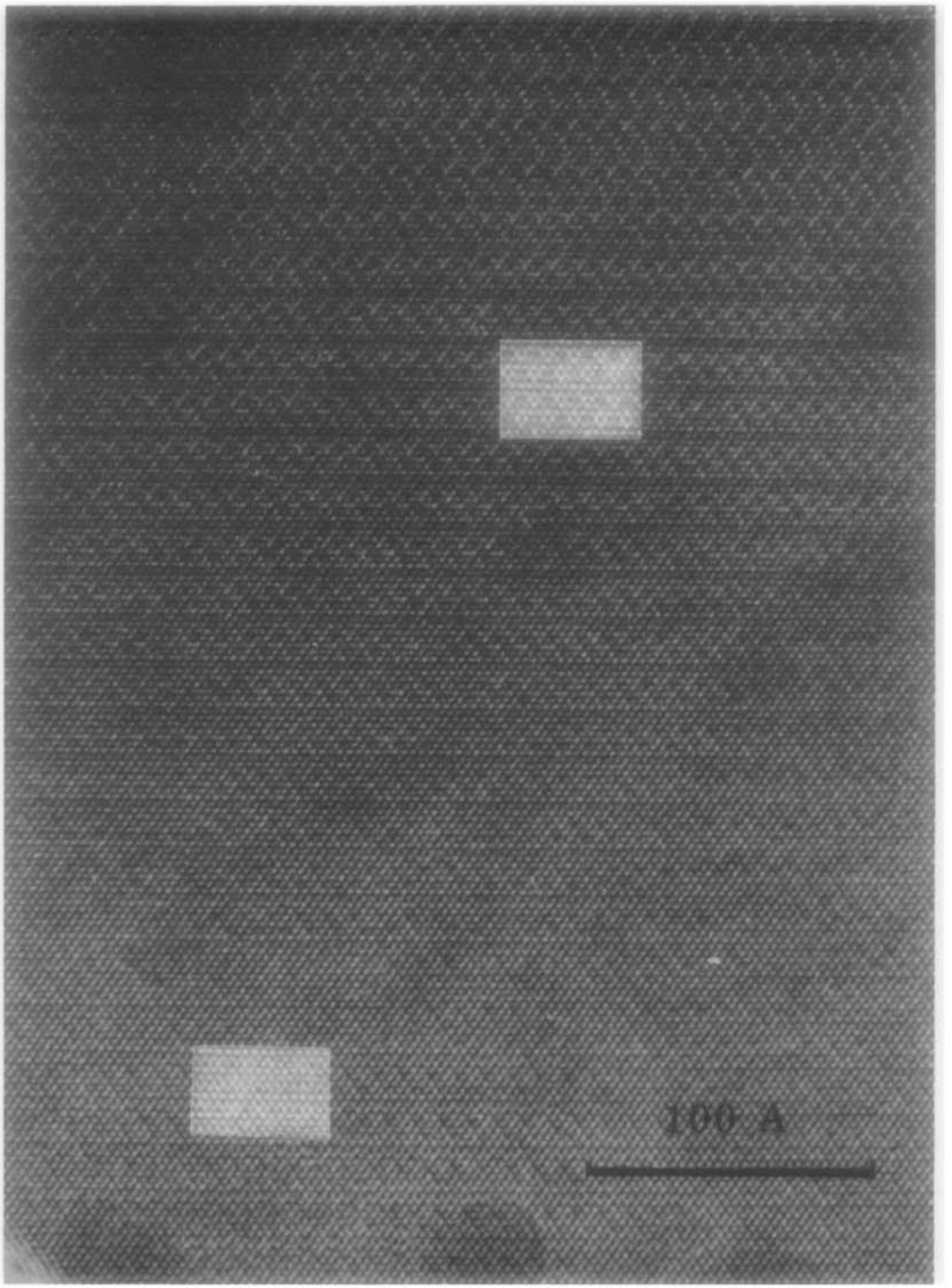

FIG. 5. Image matches for the model of Fig. 4, viewed down the [110] fluorite axis. The computer simulations correspond to 20 Å thick and a defocus of 1000 Å (near edge of crystal) and 40 Å thick and a defocus of 600 Å.

from each other by a layer consisting of bismuth and oxygen atoms only, this will increase the niobium content, as observed experimentally, and also transform the body-centered $3 \times 3 \times 7$ unit cell into a primitive $3 \times 3 \times 5$ one. This again can be confirmed by inspection of the images.

Conclusions

As with the structure of the Type II phase, the model of Fig. 4b cannot be claimed to be a unique solution of the structure. Indeed, it is possible that several structures exist with different cation arrangements which will produce the same image contrast in [110] projection. However, given the composition of the crystals, it is the only model which can take account of the valencies and known coordination preferences of bismuth and niobium. Furthermore, the incorporation of perovskite units into the structure is in accordance with the gradually increasing niobium content and the perovskite related structure of the Type IV phase (*7, 14*), and the intergrowths between pyrochlore-like phases and perovskite-related structures observed in the system Bi_2O_3–WO_3–Nb_2O_5 (*15*). Because of its construction from both pyrochlore and perovskite structural units, we believe this phase to be of significant crystal–chemical importance, as it suggests that the presently accepted clear distinction between the pyrochlore and perovskite-derived phases (*16*) may not be as absolute as hitherto suspected.

References

1. W. Zhou, D. A. Jefferson, and J. M. Thomas, *Proc. Roy. Soc. London A* **406,** 173 (1986).
2. D. J. Buttrey, D. A. Jefferson, and J. M. Thomas, *Philos. Mag.* **53,** 897 (1986).
3. W. Zhou, D. A. Jefferson, M. Alario-Franco, and J. M. Thomas, *J. Phys. Chem.* **91,** 512 (1987).
4. R. S. Roth and J. L. Waring, *J. Res. Nat. Bur. Stand. A* **66,** 451 (1962).
5. G. Galtow and D. Schuetze, *Z. Anorg. Allg. Chem.* **328,** 44 (1964).
6. A. Harriman, J. M. Thomas, W. Zhou, and D. A. Jefferson, *J. Solid State Chem.* (in press).
7. J. Gopalakrishnan, A. Ramanan, C. N. R. Rao, D. A. Jefferson, and D. J. Smith, *J. Solid State Chem.* **55,** 101 (1984).
8. B. Aurivillius, *Ark. Kemi.* **2,** 519 (1950).
9. H. P. Erickson and A. Klug, *Philos. Trans. Roy. Soc. London B* **261,** 105 (1971).
10. J. M. Cowley and A. F. Moodie, *Acta Crystallogr.* **10,** 609 (1975).
11. P. Goodman and A. F. Moodie, *Acta Crystallogr. A* **30,** 280 (1974).
12. D. A. Jefferson, J. M. Thomas, M. K. Uppal, and R. K. Grasselli, *J. Chem. Soc. Chem. Comm.*, 594 (1983).
13. E. T. Shuvaeva, *Kristallografiya* **25,** 408 (1980).
14. W. Zhou, D. A. Jefferson, M. Alaria-Franco, and J. M. Thomas (in preparation).
15. D. A. Jefferson, *Amer. Chem. Soc. Symp. Ser.* **379,** 183 (1985).
16. A. Ramanan, J. Gopalakrishnan, and C. N. R. Rao, *J. Solid State Chem.* **60,** 376 (1985).